

Intrinsic Variability and Field Statistics for the Vela Pulsar: 3. Two-Component Fits and Detailed Assessment of Stochastic Growth Theory

Iver H. Cairns, P. Das, P. A. Robinson, and S. Johnston

School of Physics, University of Sydney, NSW 2006, Australia.

arXiv:astro-ph/0304430v1 24 Apr 2003

Accepted ?? Received 2002 ??; in original form 2002 ??

ABSTRACT

The variability of the Vela pulsar (PSR B0833-45) corresponds to well-defined field statistics that vary with pulsar phase, ranging from Gaussian intensity statistics off-pulse to approximately power-law statistics in a transition region and then lognormal statistics on-pulse, excluding giant micropulses. These data are analyzed here in terms of two superposed wave populations, using a new calculation for the amplitude statistics of two vectorially-combined transverse fields. Detailed analyses show that the approximately power-law and lognormal distributions observed are fitted well at essentially all on-pulse phases by Gaussian-lognormal and double-lognormal combinations, respectively. The good fits found, plus the smooth but significant variations in fit parameters across the source, provide strong evidence that the approximately power-law statistics observed in the transition region are not intrinsic. Instead, the data are consistent with the pulsar’s normal emission having lognormal statistics whenever the pulsar is detectable. This is consistent with generation in an inhomogeneous source obeying stochastic growth theory (SGT) and with the emission mechanism being purely linear (either direct or indirect), with no evidence for nonlinear processes. A nonlinear mechanism is viable only if it produces lognormal statistics when suitably ensemble-averaged. Variations in the SGT fit parameters with phase are consistent with the radiation being relatively more variable near the pulse edges than near the center, consistent with earlier work. In contrast, Vela’s giant micropulses come from a very restricted phase range and have power-law statistics with indices (6.7 ± 0.6) not inconsistent with nonlinear wave collapse. These results are consistent with normal pulses coming from a different source and generation mechanism than giant micropulses, as suggested previously on other grounds. Analysis of field statistics thus emphasizes the richness of pulsar physics, the apparently widespread applicability of SGT, and connections between variability and generation mechanism.

Key words: pulsars: Vela; pulsars: general; radiation mechanisms: non-thermal; methods: statistical; waves; instabilities.

1 INTRODUCTION

The variability of pulsar emissions, both from pulse to pulse at a given phase and from phase to phase within a pulse, has long been unexplained (Hankins 1996). These variations include subpulses (Drake & Craft 1968), with durations of order 10 – 50% the width of the average profile and sometimes a steady drift in phase, and microstructures superposed on the subpulses (Craft, Commella & Drake 1968, Hankins 1996), which are concentrated bursts of emissions that sometimes appear quasi-periodic. The statistics of the variable fields, such as the probability distribution of fields, have not been characterized until recently (Cairns, John-

ston & Das 2001, hereafter Paper I) and few constraints have been placed on pulsar emission mechanisms, despite decades of research. This paper is the third in a series that characterizes the field statistics of pulsar variability in detail, advances interpretations in terms of existing theories for wave growth in inhomogeneous plasmas, and places constraints on pulsar emission mechanisms and the source physics. The initial analysis of Paper I, the second in the series (Paper II) [called paper II hereafter], and this paper address the Vela pulsar (PSR B8033-45), including both microstructure and subpulse effects simultaneously, while the fourth paper addresses PSRs B1641-45 and B0950+08 (Cairns et al. 2002b).

Wave growth in inhomogeneous media naturally results

in bursty, variable waves. The field statistics are determined by the intrinsic statistics of radiation generated in an individual source region (predicted by theories for wave growth in inhomogeneous plasmas, which themselves depend on the emission mechanism and physics of the source plasma), effects of spatial variations due to possible superposition of emission from multiple (sub)sources, and scattering and other propagation effects between the observer and source, as reviewed in detail in Section 2 of Paper II. Only a very brief summary is given here, with most references provided in Paper II. First, the simplest assumption is made, that the observed field statistics are determined by the intrinsic statistics of the radiation process and propagation effects. Appeals to spatial variations are warranted only if the simplest assumptions fail to match data, which is not the case here. Second, scattering is expected to produce closely-Gaussian intensity statistics (Ratcliffe 1956; Rickett 1977; Paper II), defined by equation (7) of Paper II and hereafter referred to as equation (II.7). Third, stochastic growth theory [SGT] (Robinson & Cairns 2001), corresponding to a linear instability operating near marginal stability, results in the lognormal statistics defined by (II.5). Fourth, self-organized criticality [SOC] (Bak et al. 1987), which corresponds to a strongly coupled system that is driven away from marginal stability but relaxes back via both local and system-wide events, has power-law statistics defined by (II.6) with small indices. Fifth, for non-relativistic, weakly magnetized, electron-proton plasmas the nonlinear process of wave collapse (Robinson 1997), which involves the modulational (self-focusing) instability of a wavepacket, also results in power-law statistics but with higher indices that depend on wavepacket shape and effective dimensionality. Electromagnetic simulations for the relativistic, strongly magnetized electron-positron plasmas relevant to pulsars also show collapse occurring but the field statistics were not investigated (Weatherall 1997, 1998). Since collapse is qualitatively very similar in both sets of simulations, it is presumed below that collapse in pulsar environments also leads to power-law statistics with similar indices to those for electron-proton plasmas. Sixth, nonlinear decay processes, in which a primary wave decays into product waves, cutoff the field distribution with known functional form near and above the processes nonlinear threshold. Note that SGT can coexist at moderate fields with wave collapse or decay active at higher fields.

Paper II demonstrates multiple results for the Vela pulsar. (i) The observed probability distributions $P(\log E)$ of the wave field E are well-defined as functions of the pulse phase ϕ . (ii) These distributions evolve with ϕ , from Gaussian intensity statistics off-pulse, to approximately power-law statistics in a transition region, to lognormal statistics near the pulse center, and thence back through approximately power-law statistics to Gaussian intensity statistics off-pulse again. Figure 1 illustrates this behaviour. (iii) The off-pulse data are quantitatively consistent with Gaussian intensity statistics. (iv) The field statistics near the pulse center are consistent with the lognormal form (II.5) provided analysis is restricted to fields well above the noise background. (v) However, at low E the observed $P(\log E)$ distributions lie consistently above the lognormal fit. This suggests that a second population of waves is superposed on the lognormal component.

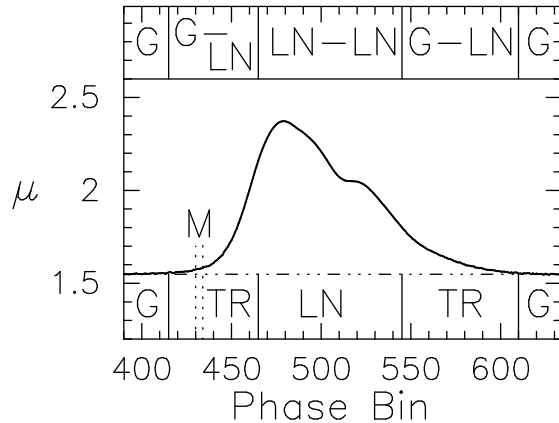


Figure 1. Vela's average pulse profile as function of phase bin, where $\mu = \langle \log E \rangle$ and the horizontal dash-dot line is the off-pulse average. At bottom symbols and vertical lines identify the transition regions (TR) between regions where the field statistics are field statistics are approximately Gaussian (G) or lognormal [LN] (Papers I & II). Vertical dotted lines and the symbol M show where giant micropulses occur (Johnston et al., 2001). At top symbols based on this work indicate where best-fits are Gaussian, Gaussian-lognormal (G-LN) or double lognormal (LN-LN).

Figure 1 also shows the restricted phase range ($\approx 430 - 434$) where Vela's giant micropulses are observed (Johnston et al. 2001; Kramer et al. 2002): defined by analogy with giant pulses (Lundgren et al. 1995), which have pulse-integrated fluxes exceeding 10 times the average pulse-integrated flux, giant micropulses have fluxes greater than 10 times the average flux at that phase. Giant micropulses and pulses are discussed further in Section 7.

Superposition of at least two wave populations is expected for the pulsar, since the Gaussian population observed off-pulse should extend on-pulse if it corresponds to measurement noise, sky background, or scattered radiation. Accordingly here we analyze the Vela data in detail in terms of two superposed wave populations, using a new theory for the statistics of two populations of transverse wave fields with known statistics that are vectorially combined together (Cairns, Robinson & Das 2002c). This theory is summarized in Section 2. The dataset is described briefly in Section 3. In Section 4 we demonstrate in detail that the approximately power-law $P(\log E)$ distributions observed in the transition regions are consistent with vector convolution of a Gaussian intensity distribution with a lognormal distribution. These fits consider almost all available data and typically have very high statistical significance. Section 5 addresses the lognormal region, showing that the combination of two lognormals provides very good fits to the available data, being demonstrably superior to the single-lognormal fits in paper I and to Gaussian-lognormal combinations. Smooth evolution in the fit parameters across the source is demonstrated in Section 6, providing additional confidence in the fits and fitting procedure. Moreover, this smooth evolution also provides an additional argument that the approximately power-law statistics seen at phases in the transition regions are not intrinsic. It is argued in Section 7 that these analyses demonstrate that the Vela pulsar's field statistics are consistent with lognormal statistics, and so SGT, being relevant. The analyses are consistent with the pulsar's emission mechanism being

purely linear (either direct or indirect) in these phase ranges, with no evidence for a nonlinear emission mechanism, consistent with our earlier analyses (Papers I & II). The results are also set in a wider context, comparing them with those for the Vela pulsar's giant micropulses and with solar system radio and plasma wave emissions. The paper's conclusions are summarized in Section 7.

2 STATISTICS OF TWO VECTORIALLY-SUPERPOSED WAVE POPULATIONS

Suppose the observed field \mathbf{E} is formed by vector addition of two fields \mathbf{E}_1 and \mathbf{E}_2 that are transverse to the measurement plane, result from different wave populations or source regions, and have separate probability distributions $P_i(E_i^2)$ for $i = 1, 2$. The probability distribution $P(E^2)$ is then defined in terms of the magnitudes E_1 and E_2 and the angle θ between \mathbf{E}_1 and \mathbf{E}_2 by (Cairns et al. 2002c)

$$P(E^2) = 2\pi A \int dE_1^2 \int dE_2^2 \int d\theta P(E_1^2) P(E_2^2) \times P_\theta(\theta) \delta(E^2 - E_1^2 - E_2^2 - 2E_1 E_2 \cos \theta). \quad (1)$$

Here $P_\theta(\theta)$ is the probability distribution for θ , A is a normalization constant, and all probability distributions are normalized by $\int dE_i^2 P_i(E_i^2) = 1 = \int dE^2 P(E^2)$. The delta function enforces the vector addition $\mathbf{E} = \mathbf{E}_1 + \mathbf{E}_2$.

Assuming that θ is uniformly distributed, meaning that the two signals are produced independently in either the same source or different regions, $P(\theta) = (2\pi)^{-1}$. Then, integrating over the θ integral using the delta function leads to (Cairns et al. 2002c)

$$P(E^2) = A \int dE_1^2 \int dE_2^2 P_1(E_1^2) P_2(E_2^2) \times |[E^2 - (E_1 + E_2)^2][E^2 - (E_1 - E_2)^2]|^{-1/2} \quad (2)$$

The square root in (2) contains integrable singularities corresponding to $\cos \theta = \pm 1$, where \mathbf{E}_1 and \mathbf{E}_2 are parallel or antiparallel. Figure 2 shows the integration domain for (2), limited by the constraint $-1 \leq \cos \theta \leq 1$ and the physical portions of the singularities (E, E_1 , and E_2 must be positive-definite). Two of the three singularity lines in Figure 2 correspond to $\cos \theta = -1$ and the factor $E^2 = (E_1 - E_2)^2$ in (2), implying that antiparallel fields \mathbf{E}_1 and \mathbf{E}_2 significantly affect the distribution $P(E^2)$. The integral (2) is performed numerically.

The $P(E^2)$ distribution is related to the corresponding intensity distribution $P(I)$ and the logarithmically-binned distribution $P(\log E)$ through their differentials and normalization conditions by

$$P(E^2) = P(\log E)/(2E^2 \ln 10) = aP(I). \quad (3)$$

Explicit expressions for lognormal field distributions and for Gaussian intensity distributions are given in equations (II.5) and (II.7), respectively.

Detailed analyses and explanations of the $P(E^2)$ distributions that result from integrating (2) over the integration domain in Figure 2 are described elsewhere (Cairns et al. 2002c). Only four of their important qualitative results are

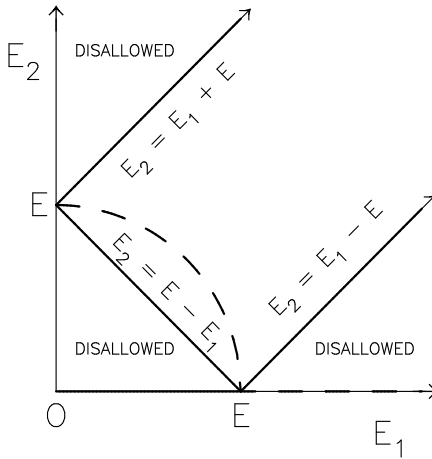


Figure 2. Integration domain for (2), the lines of singularity associated with $\cos \theta = \pm 1$ (thick solid lines), and the circle corresponding to $\cos \theta = 0$ (dashed line).

summarized here and illustrated using the $P(E^2)$ distribution predicted for two lognormal distributions in Figure 3.

First, typically, as in Figure 3, the combined $P(E^2)$ distribution, at large E above its peak, has the functional form of the individual distribution P_i that extends to higher E_i . Expected intuitively when one distribution is much more intense than the other, this result explains why previous single-component analyses were usually viable.

Second, a different functional form can be develop in the transition region between the two individual distributions. Specifically a nearly power-law form over 1 – 2 decades can result from combining a Gaussian or lognormal distribution with a lognormal distribution that is centered at lower E but extends to higher E (Cairns et al. 2002c).

Third, the prediction (2) for vectorial convolution of \mathbf{E}_1 and \mathbf{E}_2 differs markedly from the corresponding predictions for convolution of the wave intensities or field amplitudes, as illustrated in Figure 3. Accordingly, despite their familiarity and frequent use (Romani & Johnston 2001; Johnston & Romani 2002), intensity and amplitude convolution should not be used to interpret the detailed field statistics.

Fourth, vectorial combination often produces a relatively flat tail at low E below the peak of $P(E^2)$. In Figure 3 this tail clearly does not come from the individual lognormal distributions, which show very rapid falloffs, but is instead due to overlap between the P_i distributions for antiparallel vectors: since combining antiparallel vectors \mathbf{E}_1 and \mathbf{E}_2 with similar magnitudes results in $E \approx 0$, the $P(E^2)$ distribution will be significant at low E if the P_1 and P_2 distributions overlap significantly. These features are shown below to be directly relevant to the Vela data. Specifically, the power-law distributions discussed in Section 3 are due to the second effect, the first result applies primarily in Section 4, and the tail at low E is important observationally for all the Vela data. Note, via (3), the relatively flat tail for $P(E^2)$ in Figure 3 becomes an E^2 power-law for the $P(\log E)$ distribution. Only $P(\log E)$ distributions are analyzed below.

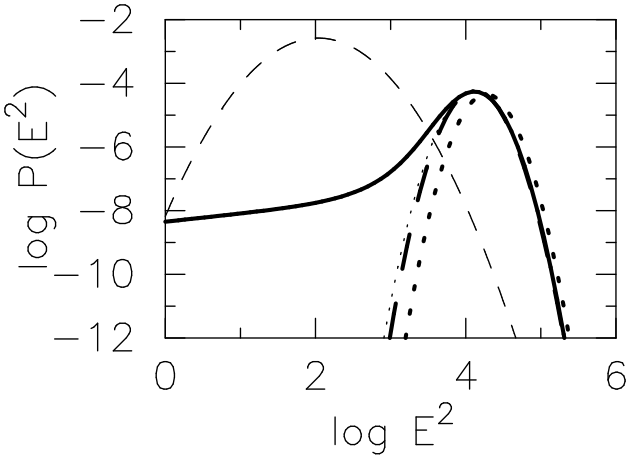


Figure 3. Distribution $P(E^2)$ resulting from vectorially combining two lognormal distributions: the thick solid line shows the combined distribution, while thick dashed and dotted lines show results for intensity and amplitude convolution, respectively, and thin dashed and dotted lines show the individual lognormal distributions. The thick dashed and thin dotted lines underlie the solid line at right.

3 DATA SET AND PREVIOUS FITS

The Vela dataset analyzed is described in detail in Paper II and elsewhere (Johnston et al. 2001, Kramer et al. 2002), so only a minimal description is given here. The radiation fields on the Parkes antenna are detected as voltages, processed via a standard backend system, and then converted into calibrated fluxes F averaged over the detector's 20 MHz bandwidth. These flux samples are recast in terms of fields and intensities to permit direct comparisons between the data and theories for wave statistics. The variables E' and I' defined by

$$E' = (F + I'_{off})^{1/2} \propto E, \quad (4)$$

$$I' = F + I'_{off} \propto I, \quad (5)$$

are related directly to the calibrated fluxes and are proxies for the incident field E and intensity I with units of $(\text{mJy})^{1/2}$ and mJy, respectively. The telescope's backend system removes the time-steady levels of receiver noise, sky and supernova background, and pulsar emission. Accordingly, an offset $I'_{off} = 1250$ mJy, equal approximately to the rms noise level off-pulse (Johnston et al. 2001, Papers I & II), is added to mitigate removal of the time-steady pulsar emission $\langle F_{psr} \rangle$, as justified in detail in paper II. Plausible causes for non-zero $\langle F_{psr} \rangle$ are (i) coherently produced radiation that undergoes scattering and diffusion as it propagates from its source, perhaps changing the phase bin at which it is observed and producing a significant background, as well as (ii) synchrotron emission from the pulsar magnetosphere or jets. Detailed arguments against this procedure and the backend system significantly modifying the true statistics are presented in Sections 3 and 9 of paper II. Note that information on both microstructure and subpulses is retained.

Figure 1 above, Figure 1 of Paper I, and Figures 1, 3–5, and 12 of Paper II show the observational context in detail. As indicated in Figure 1, and shown specifically in Figure 4 of paper II, the $P(\log E')$ distributions observed for phases 415–460 and 545–610 are approximately power-law at high

Table 1. Gaussian-lognormal fit parameters. I_0 and σ_I are in units of mJy.

Phase	μ	σ	I_0	σ_I	χ^2	N_{df}	$P(\chi^2)$
440	0.71	0.35	1804	1397	11.5	20	0.93
450	1.13	0.40	2864	1285	33.9	26	0.14
510	2.06	0.062	2633	2537	1551	15	0.00
560	0.94	0.38	2474	1334	25.9	24	0.38
590	0.68	0.40	1510	1284	18.1	21	0.65
610	0.50	0.33	1248	1380	20.6	17	0.25

E' . These distributions, in the so-called transition region, are fitted for the first time in section 4.

The $P(\log E')$ distributions observed in the approximate range 460–540 appear strongly lognormal by eye and previous single-component lognormal fits are good and have reasonable statistical significance if restricted to bins with $\geq 10^2$ counts and fields $\gtrsim 100$ (mJy) $^{1/2}$ (Papers I & II). Typically these fits accurately model the observed distribution well at fields close to and above the peak in $P(\log E')$, but lie significantly below the observations at lower E' . This latter point argues for a second component contributing to the observed distribution (Paper II), as shown in Section 4 for the power-law regions. Two-component double-lognormal fits for almost the entire range of E' are presented for phases 460–540 in Section 5.

4 TWO-COMPONENT FITS IN THE TRANSITION REGIONS

Figure 4 shows the $P(\log E')$ distribution observed at phase 440, the best fit to (2) for the combination of a Gaussian intensity distribution and a lognormal distribution, and the two individual distributions. The best fit was obtained by minimizing χ^2 for all bins with ≥ 10 counts using the amoeba algorithm (Press et al. 1986). In comparison, previous fits of similar Vela data (Paper I and II) considered only bins with ≥ 100 counts and fields $E' \gtrsim 100$ mJy $^{1/2}$ ($I' \gtrsim 10^4$ mJy) and fitted only a single component.

Excellent quantitative agreement is evident in Figure 4 between the data and best-fit curve. The fit is very good statistically: Table 1 lists the fit parameters for the Gaussian component, I'_0 and $\sigma_{I'}$ in (II.7), and the lognormal component, μ and σ in (II.5), as well as χ^2 , the number of degrees of freedom N_{df} , and the significance probability of the fit, $P(\chi^2)$. Note that good fits have $\chi^2 \approx N_{df}$ and $P(\chi^2) \gtrsim 1\%$. Comparing the Gaussian fit parameters with the properties of the off-pulse (phases 391–400) Gaussian intensity noise fitted in paper II, $I'_0 = 1215$ mJy and $\sigma_{I'} = 1420$ mJy, it is clear that the Gaussian component found here corresponds closely to the off-pulse Gaussian background and to the offset I'_{off} introduced in (5)–(5).

The best-fit line in Figure 4 is very close to the underlying Gaussian distribution except for the 4 data points with largest E' , where the data exceed the Gaussian predictions. This excess is due to the underlying lognormal distribution and corresponds to the highest E signals from the lognor-

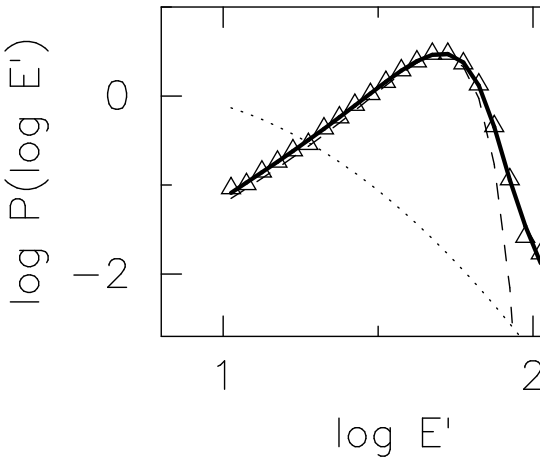


Figure 4. Comparison of the $P(\log E')$ distribution observed at phase 440 (triangle symbols) with the best Gaussian-lognormal fit (thick solid line) to the prediction (2). The dashed line shows the Gaussian distribution that is vectorially convolved with the lognormal component (dotted line) to produce the best fit.

mal adding to the Gaussian background. The simplest interpretation is that the lognormal distribution corresponds to the pulsar's intrinsic emission while the Gaussian component is a background signal. Evidence for evolution of the Gaussian background with phase is presented in Section 6 below. Thus, for phase 440, the approximately power-law form below the peak of the observed $P(\log E')$ distribution corresponds to the Gaussian background while the upturn at high E' , which develops into a power-law at larger ϕ , is due to the lognormal component.

Figure 5 shows the observed $P(\log E')$ distribution and associated Gaussian-lognormal fits at phase 450, where the observed distribution has developed closely power-law forms at both low and high E' . For reference, $P(\log E') \propto E'^{-4.1 \pm 0.5}$ at high E' and $\propto E'^{+3.1 \pm 0.3}$ at low E' and at first sight the distribution appears rather similar to theory and observations for wave collapse discussed elsewhere (Robinson & Newman 1990; Robinson 1997). Theoretical difficulties in interpreting these data in terms of collapse are described in Section 7. In contrast, the best-fit Gaussian-lognormal combination for (2) agrees very well with the observed distribution, with high statistical significance. Comparing Figures 4 – 5 and the fit parameters in Table 1, it is clear that evolution in the lognormal component explains simply the development of power-law character in the $P(\log E')$ distributions at high E' for these phases. The ensuing examples show that this interpretation is also consistent for phase bins < 440 and in the other transition region (bins 545 – 610).

Fitting the Gaussian-lognormal combination in the phase range 465 – 540, where the $P(\log E')$ distributions look strongly lognormal as shown in Section 5 and in Papers I & II, typically leads to worse fits and lower statistical significance than a double-lognormal combination. This is shown primarily in the next 2 sections, with Figure 6 shown here mostly for consistency. While Figure 6 shows reasonable agreement at high E' , the fit clearly fails for both the tail and the peak.

Consider next the transition region in phase bins 545 –

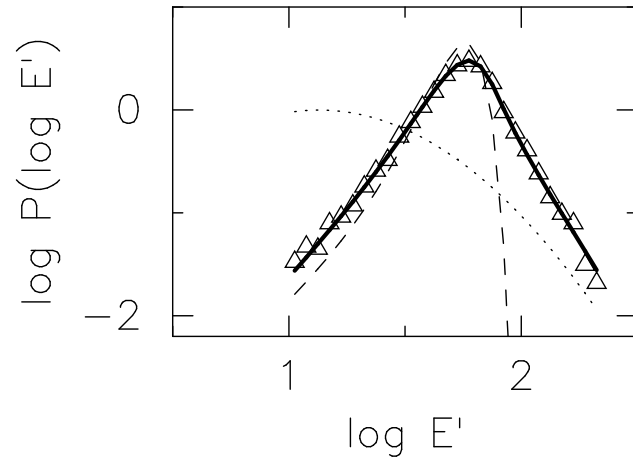


Figure 5. Comparison of the $P(\log E')$ distribution observed at phase 450 (triangles) with the best Gaussian-lognormal fit (2), using the same format as Figure 4.

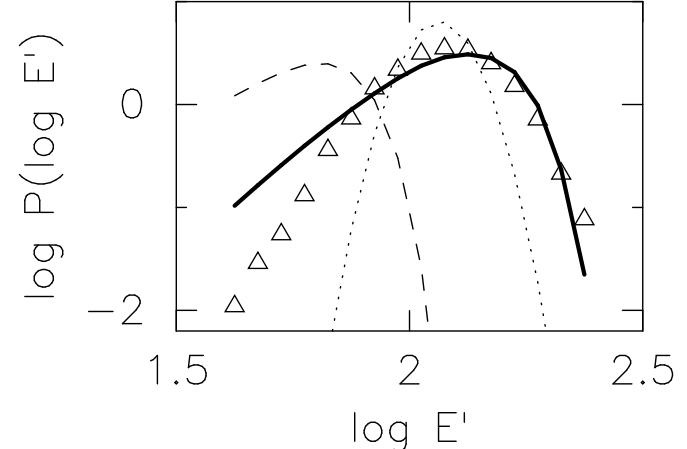


Figure 6. Comparison of the $P(\log E')$ distribution observed at phase 510 (triangles) with the best Gaussian-lognormal fit, using the same format as Figure 4.

610 where the $P(\log E')$ distributions range from being initially power-law at high E' towards being Gaussian in I' . Figure 7 shows the observed $P(\log E')$ distribution and associated Gaussian-lognormal fit at phase 560, where the distribution appears power-law both above and below its peak (indices -6.8 ± 0.9 and 2.2 ± 0.4 , respectively). Once again the agreement between the fit and data is very good, both quantitatively and in terms of statistical significance.

As the pulsar's average intensity decreases for $\phi > 560$, and so the value μ of the inferred lognormal component decreases, the power-law feature at high E' is expected to weaken and retreat into the background distribution by analogy with the results for phases 440 and 450. Figures 8 and 9 illustrate this trend for phase bins 590 and 610, respectively, and show that the observed $P(\log E')$ distributions remain very well fitted by the Gaussian-lognormal combination. The lognormal component indeed has μ decreasing with increasing phase (Table 1), while σ remains approximately constant, showing that the lognormal moves towards and below the fields characteristic of the relatively constant Gaussian component. Similar results are obtained

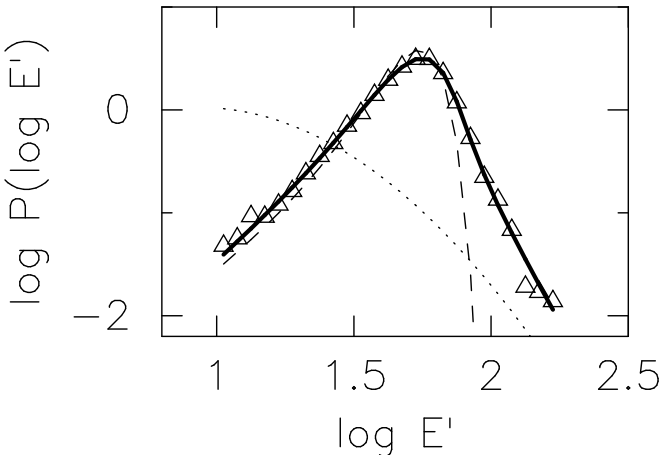


Figure 7. Comparison of the $P(\log E')$ distribution observed at phase 560 with the best Gaussian-lognormal fit, using the same format as Figure 4.

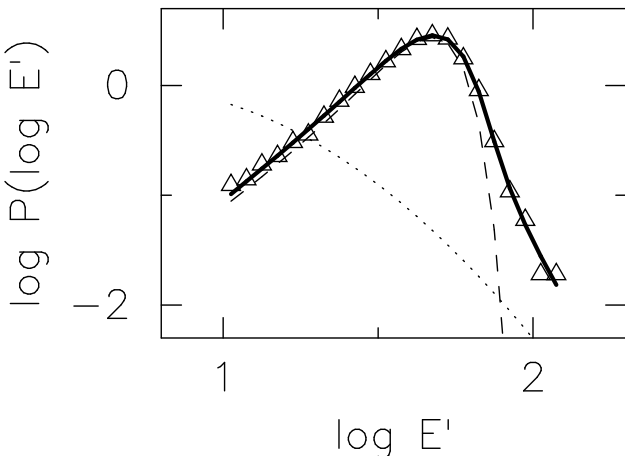


Figure 8. Comparison of the $P(\log E')$ distribution observed at phase 590 with the best Gaussian-lognormal fit, using the same format as Figure 4.

for phases 410 to 440, where the pulsar and lognormal component are moving above background.

Phase 590 (Figure 8) corresponds to the so-called ‘‘bump’’ region (Johnston et al. 2001) and shows that the bump region is not unusual, since the pulsar’s emission continues to be well described as a lognormal component. Comparison with Figure 8a of Kramer et al. (2002) emphasizes the importance of vectorial convolution of Gaussian and lognormal components via (2) for obtaining a good fit.

In summary, the fits in Figures 4 to 9 and the associated variations in Table 1’s fit parameters are strong observational evidence that the development of power-law-like features in the $P(\log E')$ distributions at high E' in phase bins 415–460 and 545–610 correspond to combination of a Gaussian background component with an underlying lognormal component of the pulsar’s emission. These power-law-like features are thus transitional stages between Gaussian intensity statistics off-pulse and strongly lognormal statistics near the pulse peak, justifying the term ‘‘transition regions’’ adopted earlier (Paper II) for these phase domains. These data therefore provide no evidence of intrinsic power-

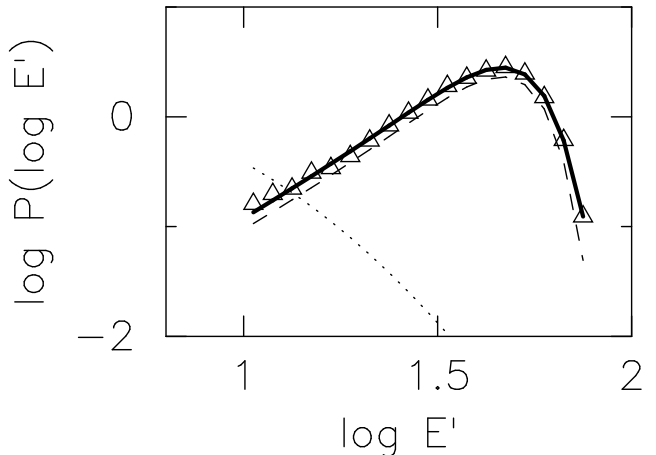


Figure 9. Comparison of the $P(\log E')$ distribution observed at phase 610 (triangle symbols) with the best Gaussian-lognormal fit, using the same format as Figure 4.

law character for the pulsar’s field statistics. In Section 7 below, it is shown that the power-law exponents for Figures 5 and 7 are inconsistent with collapse theory at low E' and at best marginally consistent at high E' . These analyses are consistent with the dominant pulsar emission on-pulse being represented well by lognormal statistics.

5 LOGNORMAL REGION AND TWO-COMPONENT FITS

For most phase bins in the range 460–540, fitting the observed $P(\log E')$ distributions with a Gaussian-lognormal combination leads to increased χ^2 and worse fits, when the fitting algorithm converges at all, than for phases below 460 and above 540. Pursuing alternatives, we found that double-lognormal fits work very well for phases 475–510, with monotonically decreasing statistical significance from phases 475 to 450 and from 520 to 550. Adequate double-lognormal fits were not found at phases below 450 or above 550.

Figure 10 shows that the double-lognormal combination works well for phase 470, which is very near the peak of the average profile (Figure 1), fitting the observed distribution well except at very low and high E' . The fit parameters are listed in Table 2. Note that the two individual lognormal distributions have very different parameters, with one centered at high E' and the other at low E' corresponding to the centroid $I'_0 = E'^2$ in (II.7) of the off-pulse Gaussian component. This is why single-component fits restricted to high $E' \geq 10^2$ (mJy) $^{1/2}$ worked well in previous analyses (Papers I & II). Similarly, at this phase fitting two components rather than one (ignoring only bins with < 10 counts) decreases χ^2 from 188 to 119 but does not improve the fit’s statistical significance qualitatively.

The results for phase 480 are excellent (Figure 11), with very high statistical significance for the fit and good agreement at all values of $\log E'$. Comparing Figures 10 and 11, the range of the $P(\log E')$ distribution narrows significantly (σ decreases) while its centroid (μ) varies relatively little. This necessarily decreases the contribution of the off-pulse (Gaussian) component to the fit. Now χ^2 decreases from 516

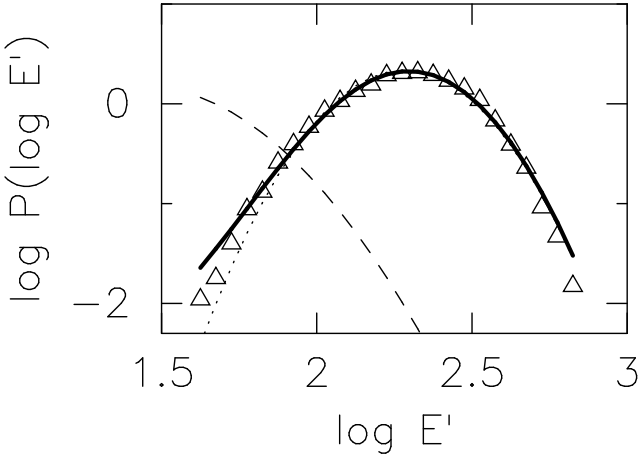


Figure 10. Comparison of the $P(\log E')$ distribution observed at phase 470 (triangle symbols) with the best double-lognormal fit to (2), using the same format as Figure 4 except that now both the dashed and dotted lines show lognormal distributions.

Table 2. Double-lognormal fit parameters, with μ_1 and σ_1 corresponding to the dominant component.

Phase	μ_1	σ_1	μ_2	σ_2	χ^2	N_{df}	$P(\chi^2)$
470	2.28	0.18	1.49	0.26	119	24	2×10^{-14}
480	2.37	0.095	1.62	0.22	5.4	15	0.99
490	2.32	0.095	1.09	0.18	44.9	13	2×10^{-5}
510	2.07	0.10	1.29	0.11	21.1	15	0.14
540	1.86	0.043	1.38	0.14	373	18	1×10^{-20}

to 5.4 for the one- and two-component fits, respectively, corresponding to a qualitative change in statistical significance. A similar result is found at phase 475.

Figure 12 presents the two-component fit for phase 490, showing it to agree very well with the data, both at large and small E' , with reasonable statistical significance. Comparing this with earlier single-component fits (Papers I &

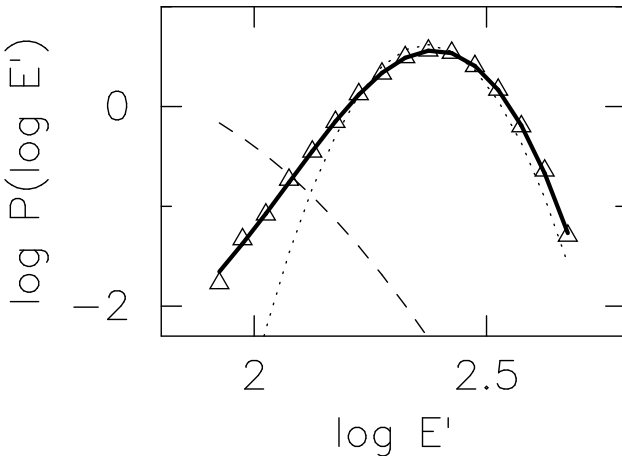


Figure 11. Comparison of the $P(\log E')$ distribution observed at phase 480 with the best double-lognormal fit, in Figure 10's format.

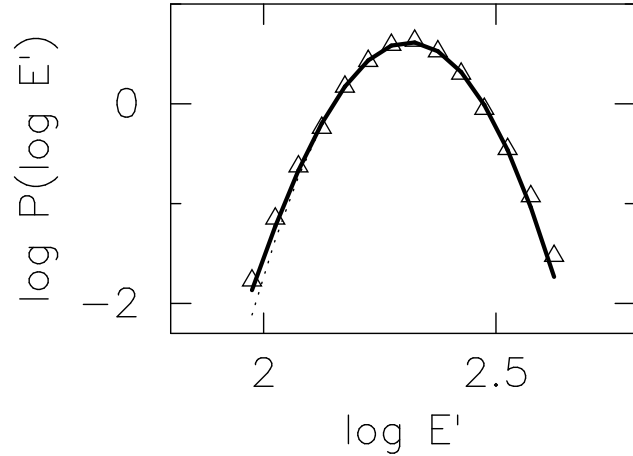


Figure 12. Comparison of the $P(\log E')$ distribution observed at phase 490 with the best double-lognormal fit, in Figure 10's format.

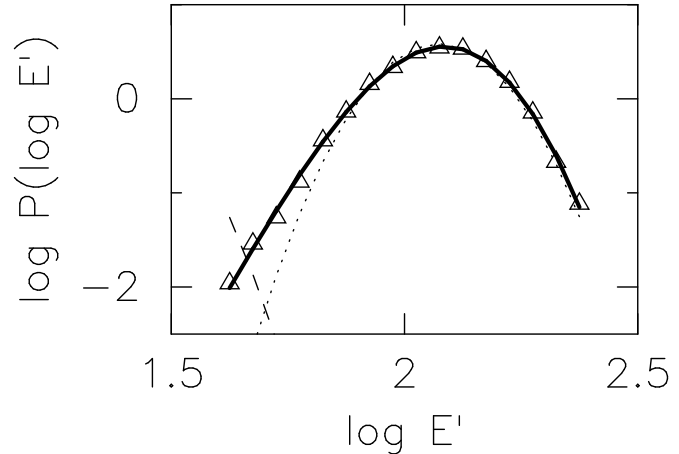


Figure 13. Comparison of the $P(\log E')$ distribution observed at phase 510 with the best double-lognormal fit (2), using the same format as Figure 10.

II), the two-component fit agrees very well with the data over a much larger domain of E' .

Figure 13 displays the double-lognormal fits for phase 510, which can be compared with the Gaussian-lognormal fit in Figure 6. The double-lognormal fits are clearly superior, correctly fitting the tail at low E' and the peak of the distribution, which were missed by the Gaussian-lognormal fit. Tables 1 and 2 show the differing statistical significances of the fits. This case demonstrates that the nature of the individual distribution (e.g., Gaussian versus lognormal) is important and an optimum choice can be discerned from the fitting results, even when the difference is primarily important for only a few data points at low E' .

6 EVOLUTION OF THE FIT PARAMETERS WITH PHASE

The Gaussian and lognormal fit parameters for the $P(\log E')$ distributions vary with the Vela pulsar's phase (Figure 14), as is evident also from comparing Figures 4 – 14 and Ta-

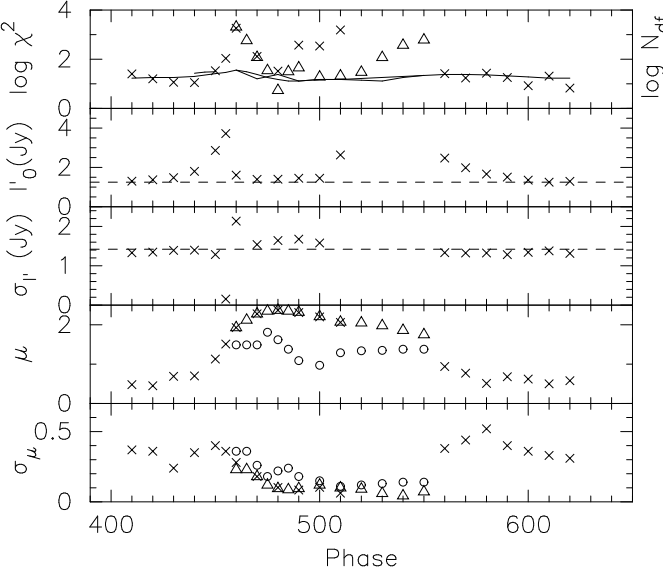


Figure 14. Comparison of the fit parameters across the source. The top panel compares χ^2 for the Gaussian-lognormal (crosses) and double-lognormal (triangles) fits with the number of degrees of freedom (N_{df}) (solid lines). The second and third panels from the top show I'_0 and σ'_1 for the Gaussian-lognormal fits. The lowest two panels show the lognormal parameters for the Gaussian-lognormal fits (crosses) and the double lognormal fits (triangles and circles).

bles 1–2. Values of χ^2 less than or approximately equal to the number of degrees of freedom N_{df} correspond to good fits from a statistical point of view. A number of important results are apparent:

(i) Either the Gaussian-lognormal or double-lognormal combinations fit the observed $P(\log E')$ distributions well at essentially all phases. Phases where only one symbol appears indicates that either no fit was found for the other combination or else the other fit had $\chi^2 \gtrsim 10^4$.

(ii) Double-lognormal fits are superior for $465 \lesssim \phi \lesssim 540$ where the pulsar's average profile peaks, while the Gaussian-lognormal combination is superior outside this domain.

(iii) The fit parameters vary smoothly with phase, except near phase bins 455 and 555 where the best-fit combinations are changing from Gaussian-lognormal to double-lognormal or vice-versa. Variations in the lognormal parameters are very large, consistent with the source plasma's parameters varying significantly with phase.

(iv) The values of μ and σ for the Gaussian-lognormal fits agree very well with those for the primary lognormal (μ_1 and σ_1) from the double-lognormal fits. This shows that a high degree of confidence can be attached both to the fitting procedures and to interpretation of the pulsar's statistics and variability in terms of lognormal field distributions.

(v) Since the primary lognormal parameters vary smoothly where the superior fitting function switches between Gaussian-lognormal and double-lognormal, these transitions primarily correspond to the functional form of the low E' wave distribution. This transition can be interpreted as evidence for evolution in the statistics of the less intense wave distribution. However, while these transitions are statistically significant, as implied by Figures 4–14, the interpretation is complicated by the fits yielding

$I'_0 \approx e^{2\mu_2} \approx I'_{off} = 1250$ mJy (Figure 14). Here μ_2 corresponds to the weaker lognormal for the double-lognormal fit. Any errors in I'_{off} thus limit the quantitative (but not qualitative) significance of fit parameters I'_0 and μ_2 .

(vi) The Gaussian component off-pulse and in the outer transition regions is best interpreted as background or measurement noise, which should be present at all phases. This is consistent with single-component Gaussian fits at off-pulse phases (Paper II) and the finding that $I'_0 \approx I'_{off}$. There is weak evidence, however, that I'_0 increases from phase bins 430 to 455 and from bins 600 to 560, in the transition regions. This can be interpreted in terms of another Gaussian component dominating or adding to the off-pulse Gaussian component in these bins, perhaps being interpretable in terms of scattered radiation or another source of radiation with Gaussian statistics. Similar evidence for evolution of the Gaussian component across the source exists for other pulsars (Cairns et al. 2002b).

(vii) The transitions from Gaussian-lognormal to double-lognormal fits and vice versa can be interpreted as evidence for a third wave component appearing near the peak of Vela's average profile and dominating the off-pulse Gaussian component and the evolving Gaussian component possibly present in the transition regions.

(viii) Finally, the bottom panel of Figure 14 shows that σ is large near the pulse edges and small near the pulse center. This is consistent with earlier statements that pulsar modulation indices behave in the same way (Taylor et al. 1975; Johnston & Romani 2002); however, the new results place the earlier statements on a much stronger physical basis, since they demonstrate that the Vela pulsar's variability corresponds to lognormal statistics and that the lognormal parameter σ varies in this way across the source, both significant steps towards developing a detailed physical model for the source plasma and emission physics. Such a model would link the wave parameters with instability physics and medium inhomogeneities, as done in several solar system contexts (Robinson et al. 1993; Cairns & Menietti 2001).

7 DISCUSSION

The existence of very good Gaussian-lognormal or double-lognormal fits to the observed $P(\log E')$ distributions at almost all on-pulse phases (excluding the giant micropulses discussed below) and the smooth evolution of the fit parameters with phase constitute very strong evidence that lognormal statistics, consistent with SGT, are relevant at all on-pulse phases for the Vela pulsar. Put another way, the pulsar's variability at all phases can be interpreted as the result of a pure SGT system coupled with a second group of weaker waves that have either Gaussian intensity statistics or else lognormal statistics. These results thus generalize and strengthen the conclusions of Papers I & II.

As remarked in Section 4, some $P(\log E')$ distributions in the transition region (Figures 5 and 7, but not Figures 4 and 9), have approximately power-law form and appear strongly reminiscent of wave collapse at first sight. On detailed examination, as shown next, the distributions are inconsistent with existing collapse theory. First, existing theory predicts that below the peak in the $P(E')$ distribution the index β (with $P(E') \propto E'^\beta$) should vary with the dimen-

sion D as $\beta = 2D - 1$ for isotropic, $2D - 3$ for prolate, and 1 for oblate collapse (Robinson & Newman 1990; Robinson 1997). Converting from the spectral index for $P(\log E')$ to that for $P(E')$ using $E' P(E') = P(\log E')$, the observed values of β are 2.1 ± 0.3 and 2.2 ± 0.4 for phase bins 450 and 560, respectively. Isotropic collapse theory predicts $\beta = 3$ and 5, for $D = 2$ and 3, while prolate collapse predicts 1 and 3, respectively. The exponents observed at low E' are thus inconsistent with collapse. Second, the indices predicted for high E' above the peak in $P(E')$, with $P(E') \propto E'^{-\alpha}$, are $\alpha = D+2$, $D+3$, and $2D+1$ for isotropic, prolate, and oblate collapse. For $D = 2 - 3$, these predictions are the integers (4, 5), (5, 6), and (5, 7), respectively. The values observed for phase bins 450 and 560 are 5.1 ± 0.5 and 6.8 ± 0.9 , respectively. While the predicted and observed ranges thus overlap for $D \geq 2$, simultaneous consistency requires oblate collapse with $D = 2$ for phase 450 and $D = 3$ for phase 560. One theoretical difficulty here is, intuitively, that strong magnetization of pulsar magnetospheres is expected to make D less than 3 (cf. Asseo et al. 1990, Asseo 1996, Weatherall 1998). Moreover, the field statistics for collapse in pulsar magnetospheres need to be investigated (cf. Weatherall 1997, 1998).

The analyses in Section 4 and the smooth evolution in fit parameters in Figure 14 thus show that the $P(\log E')$ distributions observed in the transition regions (phases 435 – 460 and 545 – 610) are best interpreted as the vectorial convolution of a lognormal component with a Gaussian intensity component and not as an intrinsic power-law component. SOC, modulational instability, wave collapse, and driven thermal waves are then inconsistent with the data. Moreover, these results show that the existence of a power-law trend in the high- E' field statistics does not automatically provide evidence for SOC, modulational instability, etc. but may instead be evidence for an SGT wave population convolved vectorially with a second population distributed as a Gaussian in I' or another lognormal (implying a second SGT wave population).

The results in Sections 4 – 6 therefore provide no evidence for an intrinsic power-law tail or for a nonlinear cut-off in the observed $P(\log E')$ distributions at high E' , which might have corresponded to nonlinear self-focusing or decay processes, respectively. This confirms, strengthens, and generalizes to almost the entire on-pulse domain earlier results for Vela (Papers I & II): the simplest interpretation is that the field statistics are consistent with the emission processes at these phases being purely linear (either direct or indirect) and inconsistent with nonlinear emission mechanisms like wave collapse (Asseo et al. 1990; Asseo 1996; Weatherall 1998). More generally, since spatial and temporal variations across the source might be important, the observations constrain viable nonlinear mechanisms to yield lognormal statistics when averaged over the ensemble of emitting structures in the source. This constraint is strong. Wave collapse, for instance, yields power-law statistics when ensemble-averaged over a homogeneous source (Robinson & Newman 1990; Robinson 1997), and so is implausible.

The origin of the second population contributing to the wave statistics on-pulse is of interest. Note that contributions from the background sky and supernova remnant are expected to be negligible due to removal of the DC offset. Where the second population has Gaussian intensity statistics, it is interpretable in terms of measurement noise (e.g.,

thermal receiver noise), scattering and diffusion of pulsar radiation, and (less probably) superposition of radiation from multiple subsources. The close similarity of the Gaussian's parameters in the outer transition regions with those off-pulse suggests that measurement noise is the most probable explanation there. Scattering is not ruled out, however, and appears to be an attractive way to interpret the increases in the Gaussian fit parameter I'_0 in the inner portions of the transition regions.

Where the second population is lognormal, it is interpretable in terms of emission from a second linear SGT system, either via a second emission process if generated in the same source as the primary population or else emission via the same or a different process in a second source region. Since the second lognormal's fit parameters are so different from those for the primary lognormal component, being restricted to fields E' close to the off-pulse background, these parameters may be contaminated by background effects. It might be tempting to suppose that only receiver noise need be considered, but the evidence for evolution in the Gaussian component for Vela (Section 6) and other pulsars (Cairns et al. 2002b) and the transitions from the best fitting function being Gaussian-lognormal to being double-lognormal (and vice versa) with phase argues against this. Finally, while the present analyses do not distinguish between subpulse and microstructure effects, analyzing both without artificial distinction, it could be that the primary lognormal component is primarily associated with microstructure physics while the second component is associated with subpulse effects, scattering, and measurement noise.

The preceding analyses and comments specifically exclude Vela's phase bins 430 – 434, where Johnston et al. (2001) observed "giant micropulses" with fluxes greater than 10 times the average flux at those phases. These giant micropulses have a cumulative probability distribution of the flux F , $\int_{-\infty}^F dF P(F)$, that appears power-law in F with index -2.85 with an associated uncertainty (by eye) $\approx \pm 0.3$ (Kramer et al. 2002). Converting into a $P(E')$ distribution using (5) yields $P(E') \propto E'^{-\alpha}$ with $\alpha = -6.7 \pm 0.6$ for Vela (Cairns 2002). Similar results are found for other pulsars with known giant micropulses or giant pulses and, moreover, this index lies within the range 4 – 7 predicted for wave collapse but lies outside the range 0.5 – 3 for known SOC phenomena (Cairns 2002). Further work on collapse theory is thus recommended for these giant phenomena, along the lines mentioned above. However, SGT also remains viable provided the power-law distributions result from vector convolution of multiple wave populations, as found in Section 4 for the Vela pulsar's normal emissions.

The foregoing results point to a richness in possible emission mechanisms and source plasma characteristics for pulsars and, more generally, for solar system and other astrophysical sources. Specifically, SGT appears to apply widely (Robinson & Cairns 2001, Papers I, II and references therein) to plasma waves and propagating radio emissions, including both Vela and other pulsars, but does not apply to all emissions. Examples include the giant micropulse and pulse phenomena discussed just above, Jovian "S" bursts (Queinnec & Zarka 2001), which have power-law flux statistics with an index of 2.0 ± 0.5 that lies in the range expected for SOC, and solar decimetric spike bursts which likely have

exponential statistics (Isliker & Benz 2001). These results show that analyses of field statistics can strongly constrain the source physics and mechanisms of natural emissions.

8 CONCLUSIONS

The variability and emission processes of the Vela pulsar can be investigated and strongly constrained using the statistics of the observed time-varying flux. The strong evolution of the pulsar's field statistics with pulse phase (Paper II), from Gaussian in the intensity off-pulse to approximately power-law in E' in the transition regions, where the average pulse profile is increasing or decreasing, and then lognormal near the peak of the average profile, show that field statistics allow probing of the source characteristics. Moreover, together with single-component fits to the pulsar's field statistics (Papers I & II), these variations are strong evidence that multiple wave populations are often superposed.

This paper presents detailed two-component fits and associated interpretations of the Vela pulsar's field statistics, analyzing microstructure and subpulse effects simultaneously, using a new prediction for the amplitude statistics of the vector sum of two transverse fields with known statistics (Cairns et al. 2002c). Excluding Vela's giant micropulses, it is shown that the approximately power-law field distributions observed in the transition regions are very well fitted by vector convolution of a lognormal with a Gaussian distribution in the intensity, the Gaussian distribution has properties very similar to the Gaussian noise observed at off-pulse phases, and the evolution with phase of the high- E' power-law form occurs as a result of the lognormal component moving relative to the background level. Accordingly, these power-laws are not intrinsic but are instead evidence for the primary pulsar emission having lognormal statistics. In the phase domain where the field statistics are strongly lognormal to the eye, double-lognormal fits are superior to Gaussian-lognormal fits, with significantly improved domains of applicability and statistical significance compared with a single-component lognormal fit. Moreover, the fit parameters for the lognormal and Gaussian distributions vary smoothly, but also significantly, with phase. Thus, at essentially all on-pulse phases the observed field statistics are very well fitted by the vector combination of a lognormal with either a Gaussian or a second lognormal. This second component may be interpreted as measurement noise, scattered radiation, or multiple superposed sources if it is Gaussian, or a second population of waves produced in a linear SGT system (either via a different mechanism in the same source or alternatively by either the same or a different mechanism in a different source region) if it is lognormal. Put another way, the Vela pulsar's emission above background is always well represented in terms of at least one lognormal. Accordingly, these results demonstrate in detail that the Vela pulsar's field statistics are consistent with SGT being relevant, and with the emission mechanisms being purely linear, whenever the pulsar is detectable above background. The pulsar's variability thus corresponds to well-defined field statistics that are consistent with emission via a linear plasma instability in an SGT state. Similar conclusions are reached elsewhere (Cairns et al. 2002b) for PSRs B1641-45 and B0950+08.

The finding that Vela's lognormal parameter σ is large

near the pulse edges and small near the center is consistent with earlier results for pulsar modulation indices (Taylor et al. 1975; Johnston & Romani 2002). These variations in σ and also μ with phase will allow future probing of the source plasma, particularly when a theory for the pulsar's SGT parameters μ and σ is developed. Finally, the richness observed in the field statistics of pulsars and of solar system emissions, plus the important constraints placed here on pulsar physics, demonstrate the power and utility of analyzing field statistics of astrophysical sources.

ACKNOWLEDGMENTS

The authors thank B. J. Rickett for helpful conversations and the Australian Research Council for financial support.

REFERENCES

Asseo E. 1996, in ASP Conf Ser. 105, Pulsars: Problems and Progress, ed. S. Johnston, M. A. Walker, & M. Bailes (San Francisco: ASP), 147

Asseo E., Pelletier, G., and Sol, H. 1990, MNRAS, 247, 529

Bak P., Tang C., Wiesenfeld K., 1987, Phys. Rev. Lett., 59, 381

Cairns I.H. 2002, ApJ, submitted

Cairns I.H., Menietti, J.D., 2001, J. Geophys. Res., 106, 29,515

Cairns I.H., Johnston S., Das P., 2001, ApJL, 563, L65 (Paper I)

Cairns I.H., Das P., Johnston S., and Robinson P. A., 2002a, MNRAS, submitted (Paper II)

Cairns I.H., Das P., Johnston S., 2002b, MNRAS, in preparation

Cairns I.H., Robinson P. A., Das P., 2002c, Phys. Rev. E, 66, 066614

Cognard I., Shrauner J.A., Taylor J.H., and Thorsett S.E., 1996, ApJL, 457, L81

Craft H.D., Comella, J.M., Drake F.D., 1968, Nature, 218, 1122

Drake F.D., Craft H.D., 1968, Nature, 220, 231

Hankins T.H., 1996, in ASP Conf. Ser. 105, Pulsars: Problems and Progress, ed. S. Johnston, M. A. Walker, & M. Bailes (San Francisco: ASP), 197

Isliker H., Benz A.O., 2001, A&A., 375, 1040

Johnston S., Romani R., 2002, MNRAS, 332, 109

Johnston S., van Straten W., Kramer M., Bailes M., 2001, ApJL, 549, L101

Kramer M., van Straten W., Johnston S., Bailes M., 2002, 334, 523

Lundgren S.C., Cordes J.M., Ulmer M., Matz S.M., Lomatch S., Foster R.S., & Hankins T., 1995, ApJ, 453, 433

Melrose D.B., 1996, in ASP Conf. Proc. 105, Pulsars: Problems and Progress, ed. S. Johnston, M. A. Walker, & M. Bailes et al. (San Francisco: ASP), 139

Press W.H., Flannery B.P., Teukolsky S.A., Vetterling W.T., 1986 Numerical Recipes. Cambridge, New York.

Queinnec J., Zarka P., 2001, Plan. Space Sci., 49, 365

Ratcliffe J.A., Rep. Prog. Phys., 19, 188

Rickett B.J., 1990, Ann. Rev. Astron. & Astrophys., 15, 471

Robinson P.A., 1997, Rev. Mod. Phys., 69, 507

Robinson P.A., Cairns I.H., 2001, Phys. Plasmas, 8, 2394

Robinson P.A., Newman, D.L., 1990, Phys. Fluids B, 2, 2999

Robinson P.A., Cairns I.H., Gurnett D.A., 1993, ApJ, 407, 790

Romani R., Johnston S. 2001, ApJ, 557, L93

Taylor J.H., Manchester R.N., Hugenin G.R. 1975, ApJ, 195, 513

Weatherall J.C., 1997, ApJ, 483, 402

Weatherall J.C., 1998, ApJ, 506, 341

Young M.D.T., Kenny B.G., 1996, in ASP Conf Ser. 105, Pulsars: Problems and Progress, ed. S. Johnston, M.A. Walker, & M. Bailes (San Francisco, ASP), 179